Construction and Building Materials 487 (2025) 142014

Contents lists available at ScienceDirect

Construction and Building Materials

journal homepage: www.elsevier.com/locate/conbuildmat

Assessment of the fracture behavior of commercial quasi-brittle gypsum boards with and without reinforced paper fibers used in timber modules

Marcus Vinícius Tavares da Costa [a,*], Borja Arroyo [b], Sergio Cicero [c]

[a] Karlstad University, Department of Engineering and Chemical Sciences, Karlstad University, Karlstad, SE 651 88, Sweden
[b] Research group EgiCAD, Depto. de Ingeniería Geográfica y Técnicas de Expresión Gráfica, Universidad de Cantabria, E.T.S. de Ingenieros de Caminos, Canales y Puertos, Santander 39005, Spain
[c] Laboratory of Materials Science and Engineering (LADICIM), Depto. de Ciencia e Ingeniería del Terreno y los Materiales, Universidad de Cantabria, E.T.S. de Ingenieros de Caminos, Canales y Puertos, Santander 39005, Spain

ARTICLE INFO

Keywords:
Gypsum plasterboards
Paper fibers
Fracture tests
Quasi-brittle fracture properties

ABSTRACT

One adopted solution for the building sector to reduce greenhouse gas emissions and fulfill the environmental requirements imposed on modern construction is the use of prefabricated timber modulus. However, gypsum plasterboards mounted in the sheathing walls of such modules are susceptible to fracture near the door openings during the on-site installation (lifting) and by horizontal loads. In this regard, fracture properties of the plasterboards are essential to be measured and integrated in structural models of the modules to predict the crack initiation and propagation toward better structural design. Here, two commercial plasterboards typically used in the timber modules, an ordinary gypsum board and a fiber gypsum board with reinforced recycled paper fibers, were evaluated under standard fracture tests for estimating the fracture properties. The fracture toughness of the fiber gypsum board (= 800 J/m^2) was twice as high as of the ordinary gypsum board (= 400 J/m^2) as well as the tensile strength evaluated at the peak forces and the traction-separation laws during the crack growth. The superior mechanical properties for the fiber gypsum board are attributed to their higher density and fiber reinforcement, and its resistance to cracking to the fiber bridging during the crack growth. Post-mortem micrographs revealed fibers almost intact with gypsum fine particles on the surfaces due to the fiber pull-out mechanism. The fracture process of the ordinary gypsum board was much affected by its paper surfacing, but a tortuous crack path was found in the gypsum core due to the significant amount of porous.

1. Introduction

Gypsum boards known as plasterboards are the pivotal building materials used primarily in ceilings, partition walls and wall coverings with relatively low cost [1]. Not only for finishing purposes the boards bring important features for buildings, such as enhanced thermal and acoustic insulation as well as fire resistance [1–4]. As being a recyclable material [5], gypsum-based materials are one of the potential materials for reducing the climate impact in the construction sector [6]. The main disadvantage of the materials is their low mechanical properties. In this regard, gypsum composites, which are gypsum mixed with different reinforcements, have been extensively studied in order to improve their mechanical performance [1]. However, there is significant variability in the reported data, which may be attributed to porosity. Gypsum composites reinforced with recyclable fibers seems to be the way forward as they offer a balance between improved mechanical properties and recyclability [7–9].

In prefabricated timber modules, for example, gypsum boards are one of key elements of sheathing walls to meet requirements of fire protection [10]. Nowadays, boards reinforced with recycled paper fibers (or simply fiber gypsum named in this study) are also used in such modules to remedy the poor mechanical performance of ordinary gypsum boards. A recent experimental investigation in full scale of different timber modules by Maharjan et al. [11] has revealed that modules assembled with fiber gypsum boards are more than twice as stiff as similar modules assembled with ordinary gypsum boards. They also found major cracks in the door openings in the boards: Modules assembled with ordinary gypsum boards were already cracked when lifted up (see in Fig. 1(a)), while modules assembled with fiber gypsum boards withstood the lifting, but they cracked as the first failure mode

* Corresponding author.
E-mail address: marcus.tavares@kau.se (M.V. Tavares da Costa).

https://doi.org/10.1016/j.conbuildmat.2025.142014
Received 7 February 2025; Received in revised form 22 April 2025; Accepted 27 May 2025
Available online 3 June 2025

caused by the shear deformation of the modules when imposing a horizontal displacement u from hydraulic pistons (see in Fig. 1(b)). Such cracks are detrimental to modular timber buildings affecting on-site installation (transportation and lifting) and safety regarding to the wind load (racking strength). The cracks lead to rework where plaster masses are used to repair them increasing the overall cost in building.

Kuai et al. [12] have investigated those cracks in walls of timber modules via experiments and developed numerical model using the extended finite element method (XFEM) to predict the ultimate capacity of the timber elements. They found that the ultimate racking strength of the timber modules can be affected up to 15 % from models with and without the ability to simulate crack growth. However, their fracture properties of the plasterboards, such as the tensile strength, fracture toughness, softening behaviour, were not experimentally determined. The uncertainties about the fracture properties could have led to another margin for the ultimate strength in their models.

The fracture properties of ordinary gypsum and fiber gypsum boards play a crucial role for the mechanical integrity and design of timber modules, in particular to the racking strength, and it has been verified in numerical structural models. However, there has been clearly a lack in experimental characterization of fracture properties of the addressed gypsum boards. From the material perspective, it is also fundamentally important to understand mechanisms behind the fracture in the boards, which cannot be unconventionally done in cumbersome structural models with many input parameters, connections and components. Understanding how the boards fracture and link it to their material microstructure are essential for optimizing the material performance that is generally lacking in knowledge in gypsum composites [1]. Therefore, the purpose of the present work is to investigate fracture properties of the ordinary gypsum and fiber gypsum boards, in the material level, by using a suitable finite element (FE) fracture modeling and standardized fracture tests. The experimental observations and the fracture properties estimated by the model here will serve to further develop the accuracy of the existing FE models of timber modules to better cover the crack initiation and propagation at the corners of door/window openings.

Gypsum boards fracture is described as quasi-brittle fracture because of the presence of the fracture process zone in front of the crack propagation [13,14]. The fracture process zone is then explained by a formation of microcracks near the initial crack tip that eventually coalesce on each other to form large cracks. Effects of aggregates also contributes in the crack formation, especially for interlocking and fricton effects [13, 15]. This material behavior has been well-described in force-crack opening diagrams [16]. As a result, quasi-brittle materials do not have an abrupt drop in force when reach the peak force (tensile strength) and rather have an exponential decay curve, viz. the tension softening behavior. One of most used models to describe the tension softening behavior is the fictitious crack model which assume that closure

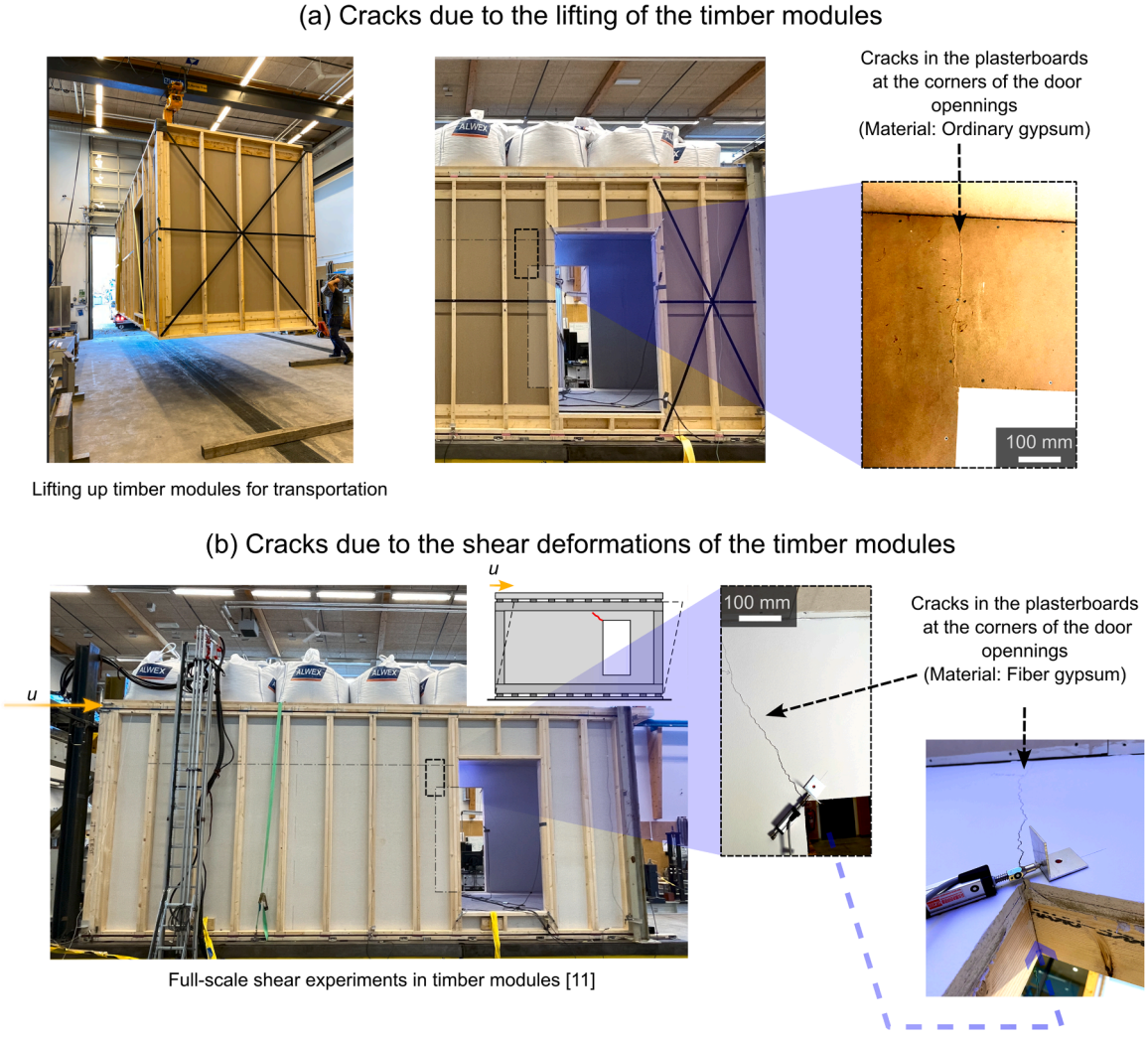

Fig. 1. Plasterboards crack at corners of door openings in timber modules in two observed scenarios: (a) Ordinary gypsum boards crack prematurely during lifting and (b) fiber gypsum boards crack due to shear deformations of the modules. The sizes of the timber modules are 7.5 × 2.6 × 3.0 m^3. (Photo courtesy of researchers MEng. Maharjan and Dr. Vessby, Karlstad University, Sweden).

tractions act in a zone near the crack tip [17–19]. This model is also well-known as the cohesive zone model, which has been implemented vastly in FE modeling for predicting fracture properties of many materials e.g. fracture toughness and the relation between tensile strength and crack openings [20]. From the reinforcements, the fibers result in materials with high toughness [21]. During the crack propagation in gypsum composites reinforced with fibers [8], the fiber bridging mechanisms dictate the fracture process where the gypsum matrix rupture and the fibers are left intact acting as bridges preventing the crack opening. The fiber bridging mechanism also soften the force-crack opening diagrams and has again been modeled with cohesive zone models e.g., in wood-based composites having the wood fibers in different orientations [22–24]. The drawback of the model is that the crack path should be well-defined beforehand.

Most recently, significant attention has been done for phase field (PF) models in computational fracture mechanics [25,26]. The modern variational model is able to predict the crack initiation and propagation by having the crack represented as a functional and having a degradation function that damages the strain energy density. PF models have the same ability of predicting complex crack propagation as conventional XFEM models, but way more efficient in terms of computational performance [27], which might have caused a boost in development of many variants of PF models recently. Wu developed one interesting variant, which includes the tension softening behavior by having the degradation function as a polynomial-like function [28,29]. Navidtehrani et al. [30] named the new version as the phase field-cohesive zone model (PF-CZM), which is capable of predicting crack initiation/propagation (PF) and the tension softening behavior (CZM). Later, the PF-CZM become even more flexible when Muñetón-Lópes et al. [31] shown that the tension softening behavior of PF-CZM can be described in different shapes by fine-tuning the coefficients and exponents of the degradation function. PF-CZM has the potential to accurately quantify fracture properties and predicting fracture of new complex materials such as fiber gypsum, but the model has only been verified over few old experimental tests in concrete as exemplified in [30,31].

In this study, the focus is primarily on understanding the fracture in commercial ordinary gypsum and fiber gypsum boards used in timber modules by four-point single-edge-notched bending tests (4SENB) coupled with digital image correlation (DIC) for monitoring the fracture development and thus obtain force-crack opening diagrams. This work also explored the ability of PF-CZM to capture the crack propagation in two loading scenarios and to curve fitting the diagrams to obtain fracture properties of fiber gypsum. This was enlightened by conducting the tests in two experimental setups: symmetric and asymmetric bending that drives the crack paths. In addition, porosity is measured by microtomography and details of fracture surfaces are examined by microscopy for both materials.

2. Materials and methods

2.1. Materials

In this investigation, two types of gypsum boards were studied: An ordinary gypsum board (Classic board, Knauf Sverige GmbH, Sweden) and a fiber gypsum board (Fermacell, Germany). The ordinary gypsum boards are typically produced in steps as: (i) Pre-drying gypsum to create the stucco, (ii) mixing the stucco with additives, (iii) pouring the slurry (mixture) with controlled speed on a paper liner, (iv) covering the slurry with a second paper liner, and finally, (v) cutting and (vi) drying the assembly in an oven to form the boards [32]. The material composition is gypsum and calcium carbonate (> 93 %), paper (2–6 %) and additives of organic surfactants, cementitious materials, glass fibers and silicones (<1 %). For the fiber gypsum boards, the production steps are quite different as: (i) Pre-shredding waste paper in a special shredding machine, (ii) defibrillating the pieces in a fiber mill to obtain the paper fibers, (iii) mixing dry gypsum powder, the paper fibers and water to form the slurry, (iii) pressing, (iv) drying the slurry, and finally (v) sanding it to the target thickness and cutting [33]. Here, the mixing and pressing steps are crucial for the mechanical performance of the final boards. The mixing step guarantees homogeneous distribution of the paper fibers resulting in an isotropic material. The pressing step, under very high pressure, pushes the air and excess water out of the slurry, which results in higher density boards compared to the ordinary gypsum boards. The material composition is gypsum and calcium carbonate (80–85 %) and recycled paper fibers (15–20 %); the fiber composition is simply regarded as recycled cellulose fibers from post consumer waste paper and recycled water. Typically, the recycled cellulose fibers have the width of ≈ 15–20 μm and length of ≈ 1–5 mm [34–36]. Fig. 2 shows photographs of the materials where both boards have the same thickness of B= 12.5 mm.

For the tests, sixteen samples each material were cut from the boards with a table saw (Robland NX 310, Belgium) in dimensions related to the thickness of the boards as $W\times$ 5 W where the height W is twice as the thickness of the boards W= 2B; the sample's front view is shown in Fig. 2 (b). The samples were then weighted for evaluation of densities before notching. After, an initial notch of width of 2 mm was made in the samples with a bench circular saw (Proxxon, Germany). The notches were sharpened manually with a knife blade for the initial crack tip. Fig. 2(c) shows the final sharp notch in a fiber gypsum sample. For DIC measurements, the surfaces of the samples were painted in white and black speckled with can spray paints (Würth, Germany). Before the tests, all samples were conditioned in a constant-climate laboratory at 20 °C and 65 % relative humidity for at least 24 h.

2.2. Four-point single-edge-notched bending tests

A customized four-point bending rig was manufactured to accommodate the samples as shown in Fig. 3(a). Two types of experimental setups for 4SENB tests were conducted where four samples each material were sorted out each test type: The experimental setup I in Fig. 3(b) of which induces pure mode I fracture and the experimental setup II (viz. asymmetric four-point tests [37]) in Fig. 3(c) of which the crack is subjected to constant shear forces — for practical reason, wooden spacer was positioned between the samples and supports in the setup II to avoid local damage. The first, which provides stable crack growth along the initial notch plane [38], is intended to determine the fracture properties of the studied materials. The second provides interesting crack propagation paths despite the constant shear forces [39,40]. Here, the experimental setup II was therefore used to verify whether the FE model is able to predict the crack propagation path using the fracture properties from experimental setup I. The tests were carried out in a uniaxial testing machine (MTS Exceed E43, USA) with the displacement control mode of speed of 1 mm/min. The force F was measured by a force transducer of capacity of 5 kN. Having the maximum force in the experimental setup I allows to estimate the tensile strength from the beam theory as

$$\sigma_{\max} = \frac{M_{\max}}{I} y = \left\{ M_{\max} = \frac{F_{\max}}{2} W, y = \frac{W-a}{2}, \quad I = \frac{B(W-a)^3}{12} \right\} = \frac{3F_{\max} W}{B(W-a)^2} \tag{1}$$

where a is the initial crack length of size of B. The span to depth ratio of the tests followed the recommendations of the standard ASTM E1820 [41]. The experimental apparatus used in the fracture tests is shown in Fig. 3(a).

During the tests, a scan camera (JAI GO-5000M-USB, Denmark) with industrial lenses (Kowa LM16HC, Japan) was positioned in front of the samples to record test frames with a framerate of 1 frame per second (FPS). After the tests, the sequential frames were imported to a DIC

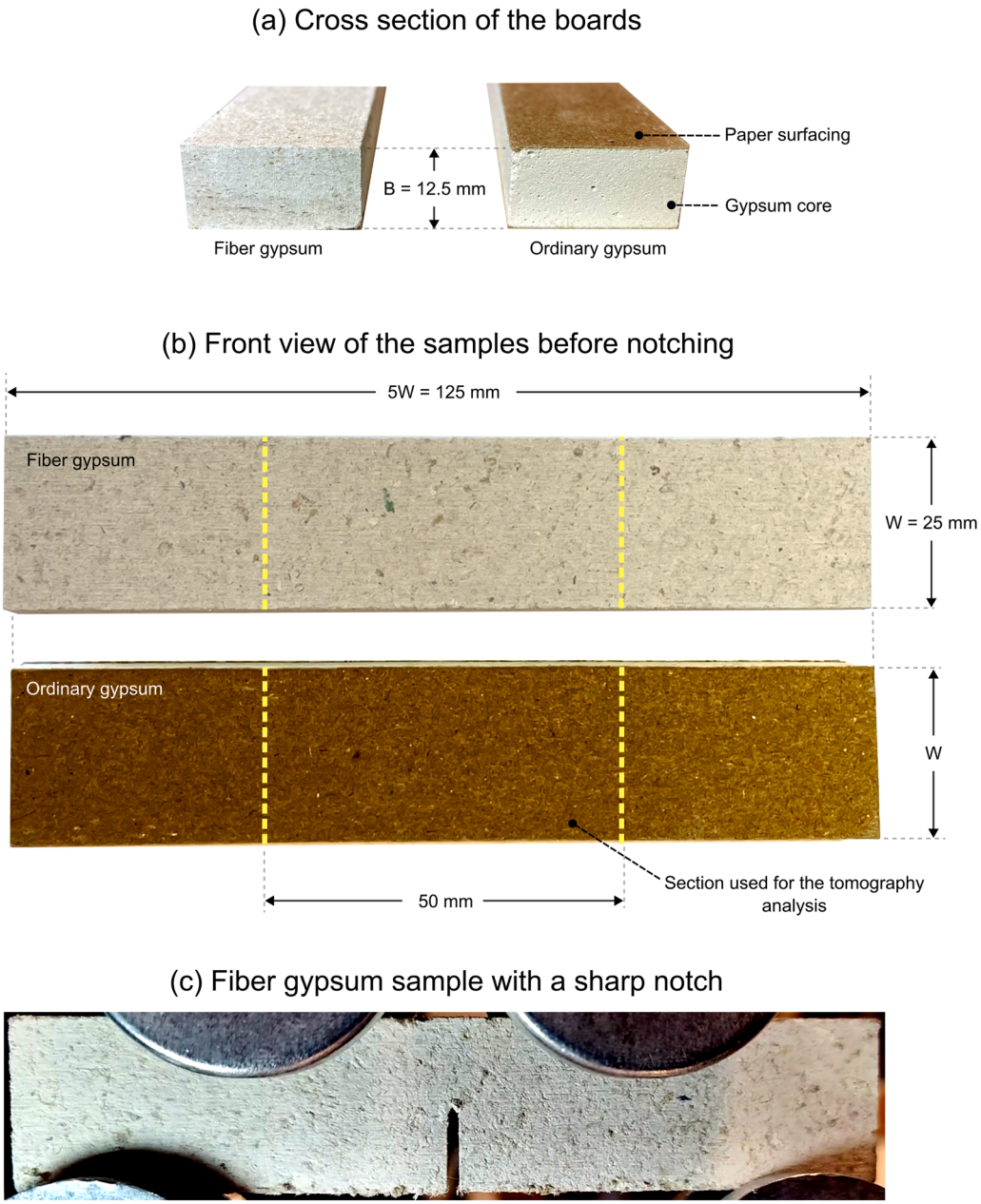

Fig. 2. Photographs of the materials: (a) Cross section of the boards, (b) front view before notching, and (c) a fiber gypsum sample with a sharp notch for the fracture test.

software (GOM, Germany) for calculating the strain fields and displacements near the crack tip. With the DIC results, the effective crack opening displacement Δ_{eff} was measured between two virtual gauge points A and B near the crack tip as illustrated in Fig. 3(b-c). The effective crack opening displacement was determined as the norm between the points as

$$\Delta_{eff} = \sqrt{\left(\overrightarrow{\mathbf{AB}}_x - 4\text{mm}\right)^2 + \left(\overrightarrow{\mathbf{AB}}_y\right)^2}. \quad (2)$$

2.3. FE model with the phase field-cohesive zone model for fracture

To assess the fracture properties as well as the crack propagation and Δ_{eff}, FE models were developed for both setups in the FE software ABAQUS. The models, named FE model I and FE model II, are in the plane state of strain whose boundary conditions and meshing are shown in Fig. 3(d-e). The refined mesh near crack has the size of 100 μm, which provides relatively no change in solution regarding mesh sensitivity. The rollers were modelled as rigid arcs where fixed boundary conditions were set at the reference nodes in the bottom ones and prescribed vertical displacement u set in the upper ones in the same way. Contacts between the rollers and other parts were frictionless as they are rotation free along their one axis in the bending rig. At middle top node of the samples, horizontal displacements were set to zero to impose symmetry and avoid any convergence problems. For the FE model II, the wooden spacer was defined as orthotropic linear elastic material because plywood pieces were used in the experiments where their elastic properties were found in [42]. Their mesh refinement was to avoid any interpenetration between elements with the sample part. The contact interaction between the spacer and the sample part had a friction coefficient of 0.3.

Here, the fracture was modelled with PF-CZM over the whole domain of the sample parts Ω where the total potential energy is defined as [28, 29]

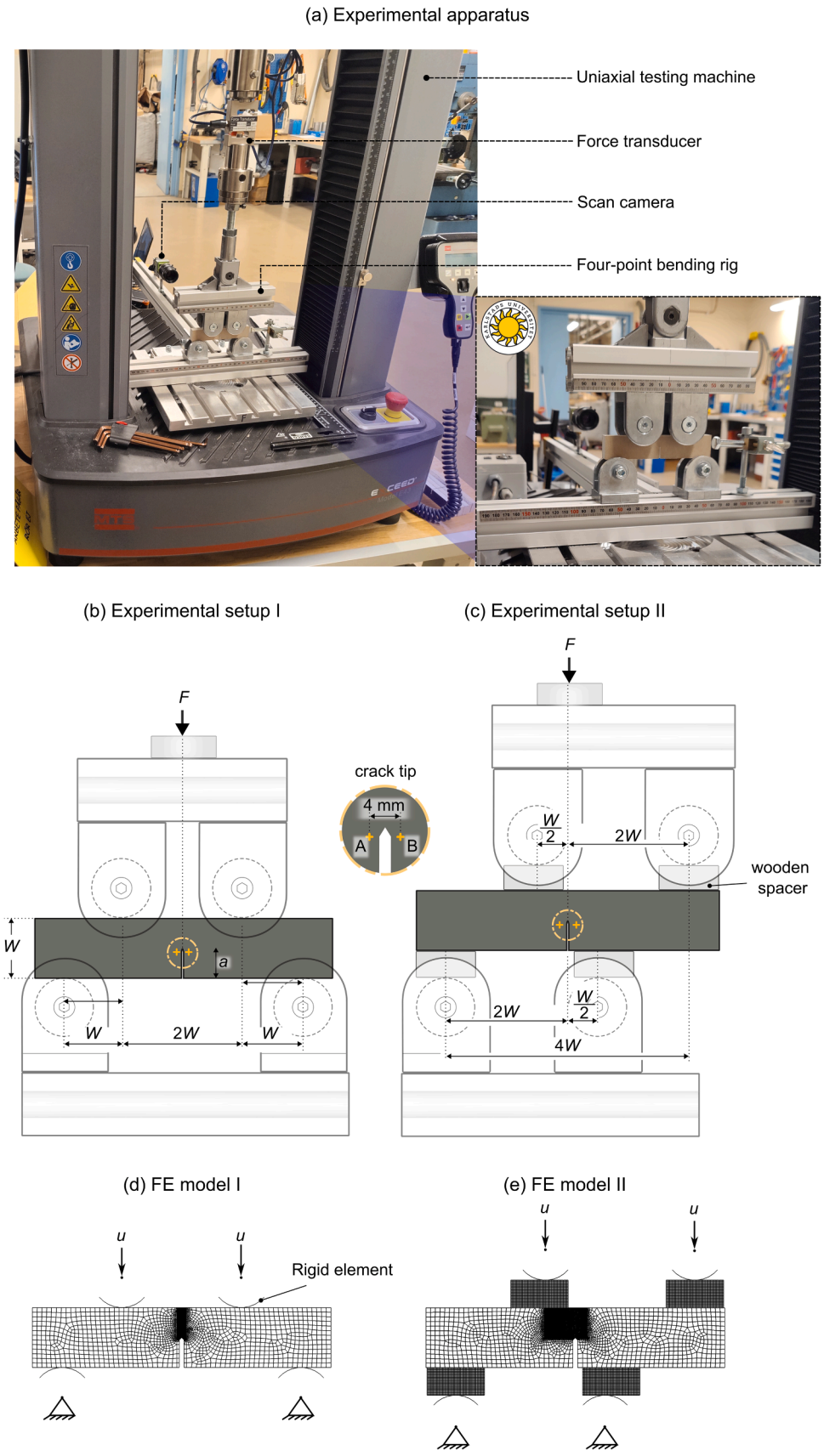

Fig. 3. (a) Experimental apparatus and (b-c) setups for the fracture tests. (d-e) Geometry, meshing and boundary conditions of the FE models.

$$\Pi(\boldsymbol{\varepsilon}, d) = \omega(d)\psi(\varepsilon) + \frac{G_c}{c_0}\left[\frac{\alpha(d)}{l_0} + l_0|\nabla d|^2\right] \text{ in } \Omega \tag{3}$$

where the first term in the right-hand side accounts for the degradation of the strain energy density $\psi(\varepsilon)$ by a polynomial-like function as

$$\omega(d) = \frac{(1-d)^p}{(1-d)^p + Q(d)}, Q(d) = a_1 \bullet P(d) = a_1 d + \quad a_1 a_2 d^2 \tag{4}$$

where d is the phase field damage variable that spans in a range between zero (intact material) and one (fully cracked material). The model coefficient $a_1 = \frac{4}{\pi l_0}\frac{EG_c}{\sigma_{max}^2}$ is estimated by knowing the elastic modulus E, fracture toughness G_c, tensile strength σ_{max} and length scale parameter l_0 of the material [28]. In this study, length scale parameter is set as $l_0 = \frac{W}{100}$ similarly elsewhere [31]. The interesting parameters a_2, and p determine the tension softening behavior. This can be evaluated by a simple parametric study using the analytical solution for one-dimensional bar under tension of PF-CZM [29,31]. The influence of a_2, and p are shown in Fig. 2 in a normalized form where the normal traction

$$T_n(d) = \sigma_{max}\sqrt{\frac{(2-d)(1-d)^p}{2P(d)}} \tag{5}$$

is plotted against the normal crack opening

$$\Delta_n(d) = \frac{4\sqrt{2}G_c}{\pi\sigma_{max}}\int_0^d \left[\frac{P(d)}{(1-d)^p}\frac{2-\beta}{2-d} - \frac{P(\beta)}{(1-\beta)^p}\right]^{-\frac{1}{2}}\frac{P(\beta)\sqrt{\beta}}{(1-\beta)^p}d\beta. \tag{6}$$

As observed by Muñetón-Lópes et al. [31], the parameter a_2 controls the initial slope during the softening and p controls the shape of the softening; The properties in Fig. 4 were unity inputs.

The second term in the right-hand side in Eq. (4) is the crack density functional, which allows to represent discontinuous cracks as smeared cracks [26]. There, the geometric function of the crack is $\alpha(d) = 2d - d^2$ and the scaling function is $c_0 = 4\int_0^1 \sqrt{\alpha(s)}ds$.

PF models are quite stablished models in computational fracture mechanics whose numerous previous works have already dissected their solution procedures with their FE implementations in open and commercial FE packages. By convenience, we explored the user material type (UMAT) subroutines developed by Navidtehrani et al. [30] and therefore direct the readers to their publication for further details of the FE implementation. The calculation in this study were performed with the staggered scheme and the hybrid spectral strain energy split for more computationally efficient performance [25].

2.4. Tomography, fracture surfaces and microstructure

Porosity is one of the main detrimental factors that affects the mechanical performance of gypsum materials and is important to correlate it to measured mechanical properties [43]. For quantifying porosity in this work, new small samples with lengths of 50 mm were cut from two reference samples without notch. Fig. 2(b) shows the middle section where the small samples each material were from. The small samples were brought to a micro-computed axial tomography (μ-TAC, Bruker Skyscan 1172, Germany) operating in parameter setting as voltage of 80 kV, current of 100 uA, exposure time of 10000 ms, rotation step of 0.2 associated with an Al+Cu filter to obtain three-dimensional (3D) scans; the detail detectability achieved was 1 micron, which may be taken as the void diameter boundary used in the characterization in practice. The scans were processed with the 3-phase method (binarization, despeckle and analysis) in the bruker software [44]; After the scans and 3D reconstructions, some isolated voxels were cleaned by using a despeckle filter; Then, the voids (porous) and solid materials were distinguished in grayscale image segmentation of which volume of porous could be calculated.

To understand the fracture processes after the 4SENB tests, some samples were split up at cracks and had their fracture surfaces examined by a field-emission scanning electron microscope (SEM, ZEISS EVO MA 15, Germany). Fractography would provide more details of the crack front, microstructures features and other elements. Ordinary optical microscopy was also used to complement the observations, in particular the crack path.

3. Results and discussions

3.1. Pre-peak force mechanical response

Fig. 5 shows the force as a function of Δ_{eff} until the peak forces in the experimental setup I and experimental setup II. Both materials noticeably performed better in the shear loading case (setup II) with 5–7 times higher in peak forces than in the bending loading case (setup I). The fiber gypsum board is remarkably stronger than the ordinary gypsum one reaching the measured forces of 1.7 times higher than in the ordinary gypsum board for setup I and approx. twice as higher for setup II; The averages of peak forces are reported in Table 1. This difference in withstanding forces can be attributed to the difference in densities where density of the fiber gypsum board is also 1.7 higher than of the ordinary gypsum material as shown in Table 1. Typically, reducing the density of gypsum boards to target lightweight causes a reduction of the mechanical strength [45].

Initial stiffnesses K_0, estimated until approximately 0.015 mm of

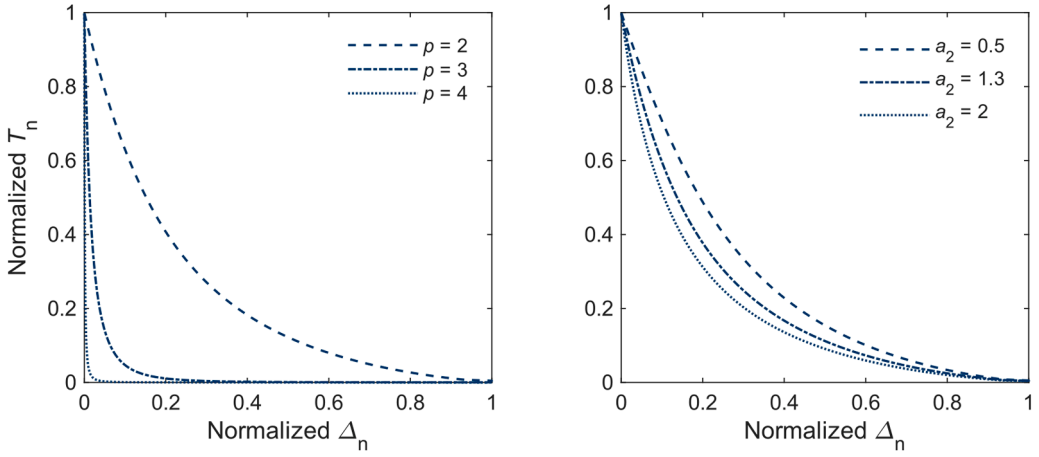

Fig. 4. Shapes of the tension softening behavior of different exponents p (left) and different coefficients a_2 (right).

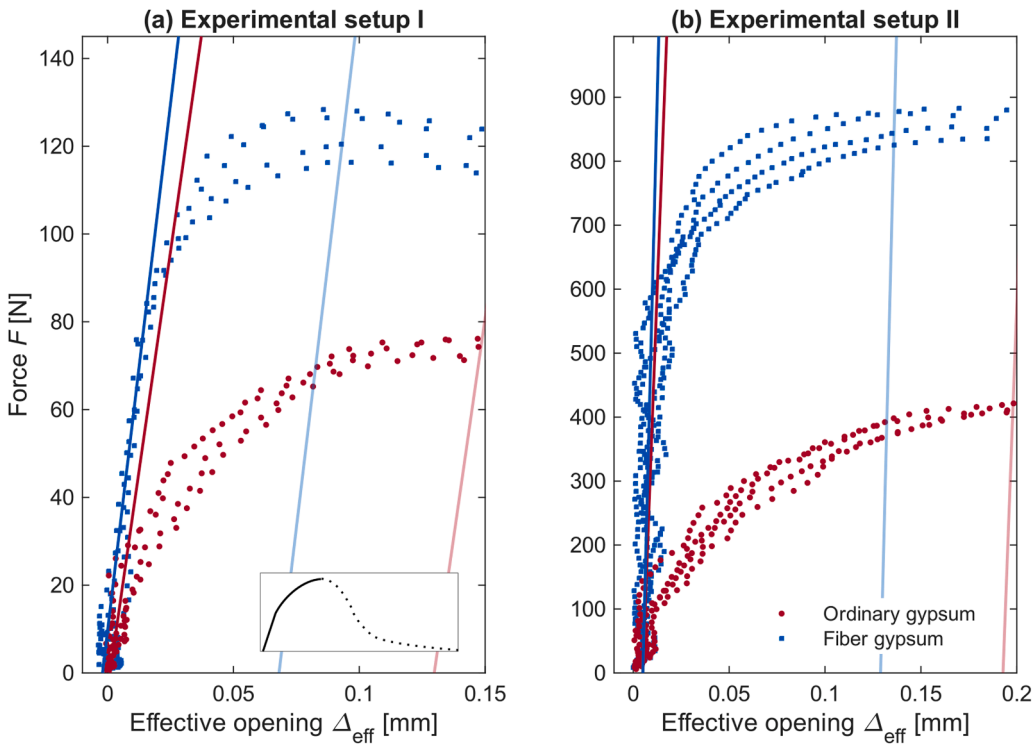

Fig. 5. load-crack effective opening curves from the initial stage until the peak force for (a) the setup I and (b) setup II.

Table 1
Experimental results from the experimental setup I and II.

Material	Exp. setup	Density* ρ [kg/m^3]	Porosity [%]	Initial stiffness K_0 [kN/mm]	Effective opening pre-peak force Δ_{eff}^{PPF} [μm]	Peak force $F_{max} \pm$ (SD) [N]
Ordinary gypsum	I	696	28	4.0	130	74 ± 2
	II			80.0	190	417 ± 8
Fiber gypsum	I	1155	19	4.8	65	123 ± 6
	II			120.0	130	860 ± 20

* Densities of the samples calculated as masses of prismatic samples without notch over their volumes.

effective opening, are higher for the fiber gypsum board in both setups with 1.2 times higher for setup I and 1.5 times for setup II. In all tests, the samples showed a nonlinear response before peak force as typically seen in rock-like materials [15]. The nonlinearly is often related to development of microcracks near the crack tip in rock-like materials [13,14]. In case of the ordinary gypsum, the ductility of paper surfacing is also included. The nonlinear behavior was quantified as effective openings pre-peak force Δ_{eff}^{PPF} by using the offset method measuring the horizontal distance between the slopes at initial and peak force locations. For both materials, Δ_{eff}^{PPF} in setup I was larger than setup II and ordinary gypsum displaced more nonlinear behavior than fiber gypsum before peak force.

3.2. Crack growth and tension softening behavior

The complete force-Δ_{eff} curves for all tests are shown in Fig. 6. For experimental setup I, both materials displayed exponential softning behaviors with stable crack growth until $\Delta_{eff} \approx 2$ mm where the tests were aborted. For cementitious materials, the first drop (zone 1–2) are described as zone where microcracks accumulate and coalesce in each other and the subsequent large tail (zone 2–3) are results of aggregate interlocking and fricton effects [13,15]. However, this phenomenon is not entirely for the ordinary gypsum board because the tension softning behaviour was much attributed to the paper surfacing. Fig. 7(a) shows the first principal strains for representative samples to illustrate the crack growth during the tests where the 1–2–3 labels correspond to

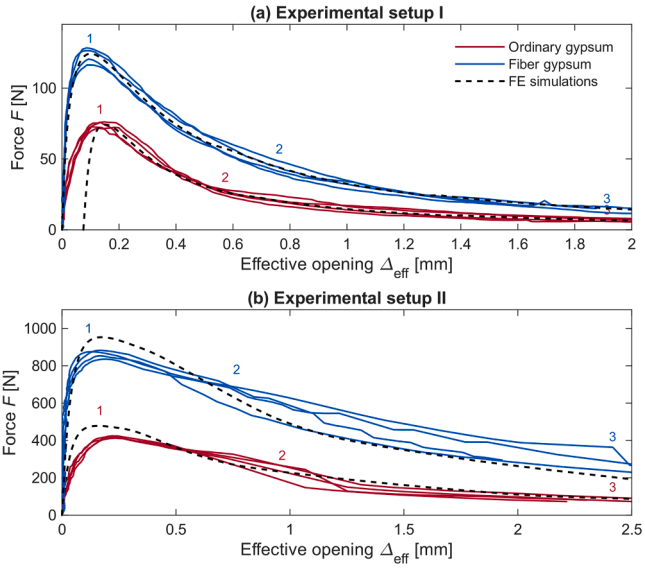

Fig. 6. Complete load-effective crack opening curves from (a) the setup I and (b) II.

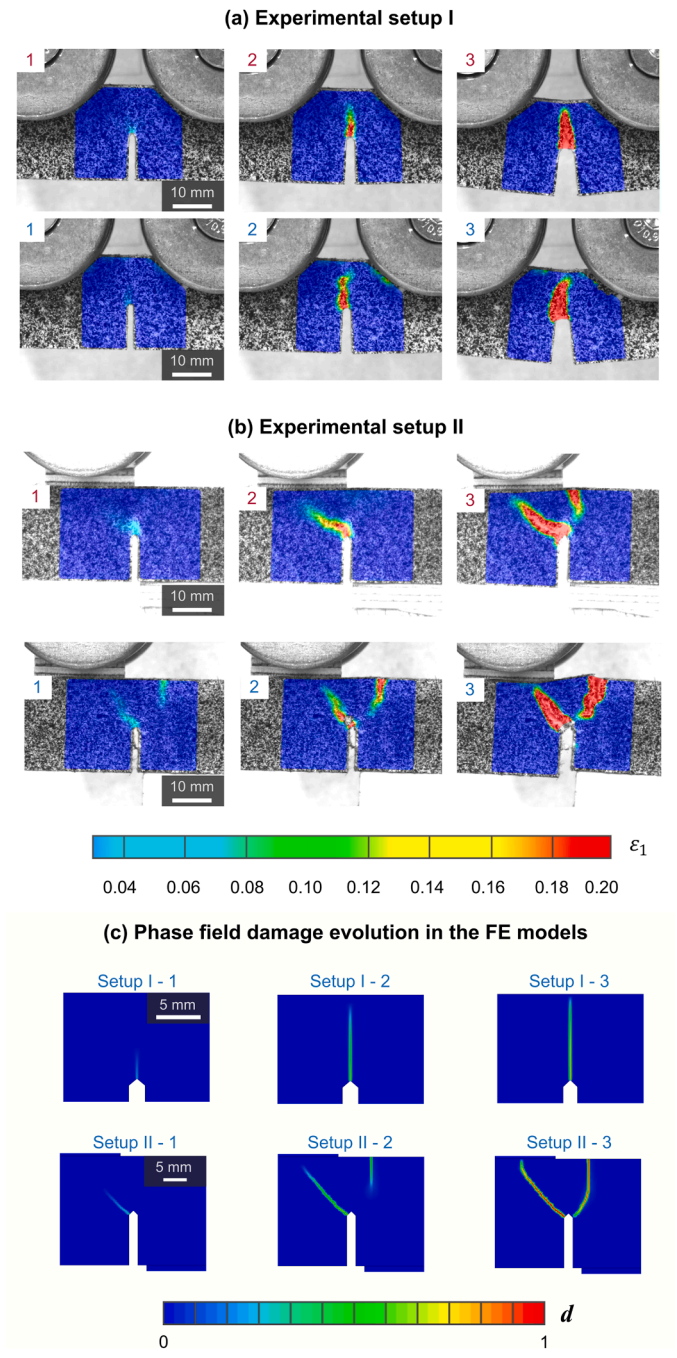

Fig. 7. Crack propagation from the experimental setups (a) I and (b) II measured by the first principal strain ε_1. (c) Same crack propagation was found by the evolution of the phase field damage d in the FE models.

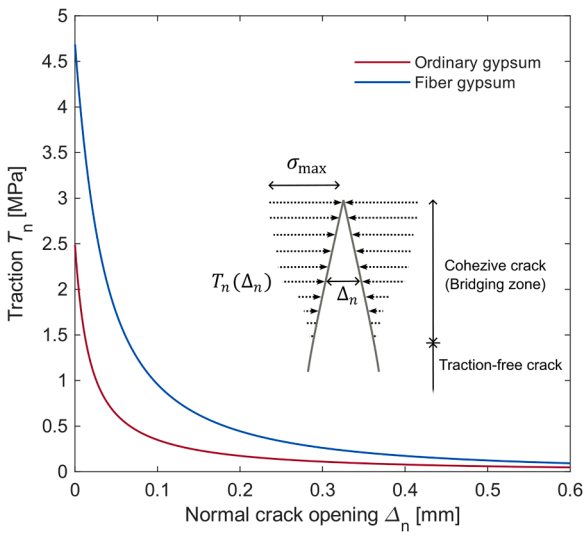

Fig. 8. The traction-separation laws for the tension softening behavior of the materials with a representation of the idealized fracture process zone.

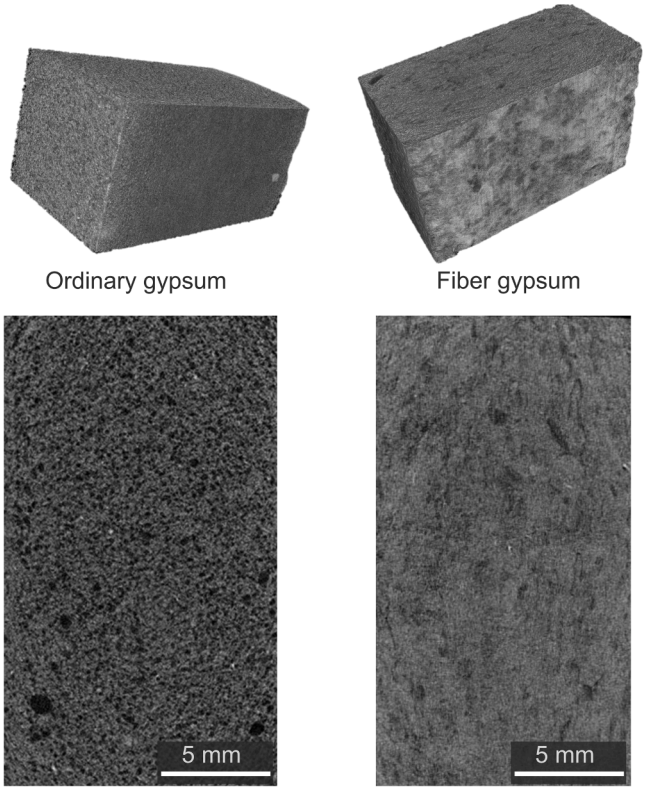

Fig. 9. Tomography scans from the reference samples; left: ordinary gypsum and right: fiber gypsum.

different stages and legend colours in Fig. 6 for the tension softening behavior. The strain developes relatively elongated for both materials, which tipically relembles the shape of the fracture process zone in quasi-britlle materials [13]. For the ordinary gypsym board, this is also the fracture process zone related to paper fracture, which is typically in the size of few millimeters corresponding to a distance comparable to the paper fiber length [46].

The crack growth of the fiber gypsum board are straghter than of the ordinary gypsum board (see photographs in Fig. 10 (a, b)). The ordinary gypsum samples have paper surfacing on their faces that had masked the tortusity of the fracture path in the gypsum core (conf. Fig. 10 (a, c)); Fig. 10 (a) shows the crack in the paper surfacing and the crack in the gypsum core by fine griding the paper. For the experimental setup II, the force drop from peak force to final sampling forces ($\approx \Delta_{eff} = 2.5$ mm) was not pronounced as it was for setup I as shown in Fig. 6(b). However, the tension softning behaviour exhibited more scatter among the tested samples because of the presence of two cracks. Fig. 7(b) shows the formation the cracks: the first crack formed at the initial crack tip are typical shear cracks that propagates diagonally; although it is pure shear setup the crack does not propagate in the direction of the loads because cementitious materials are weak in tension and therefore the crack path goes towards in-plane principal stresses [47]. The second crack occurred when the extention of the first crack had passed the righ-hand side of the

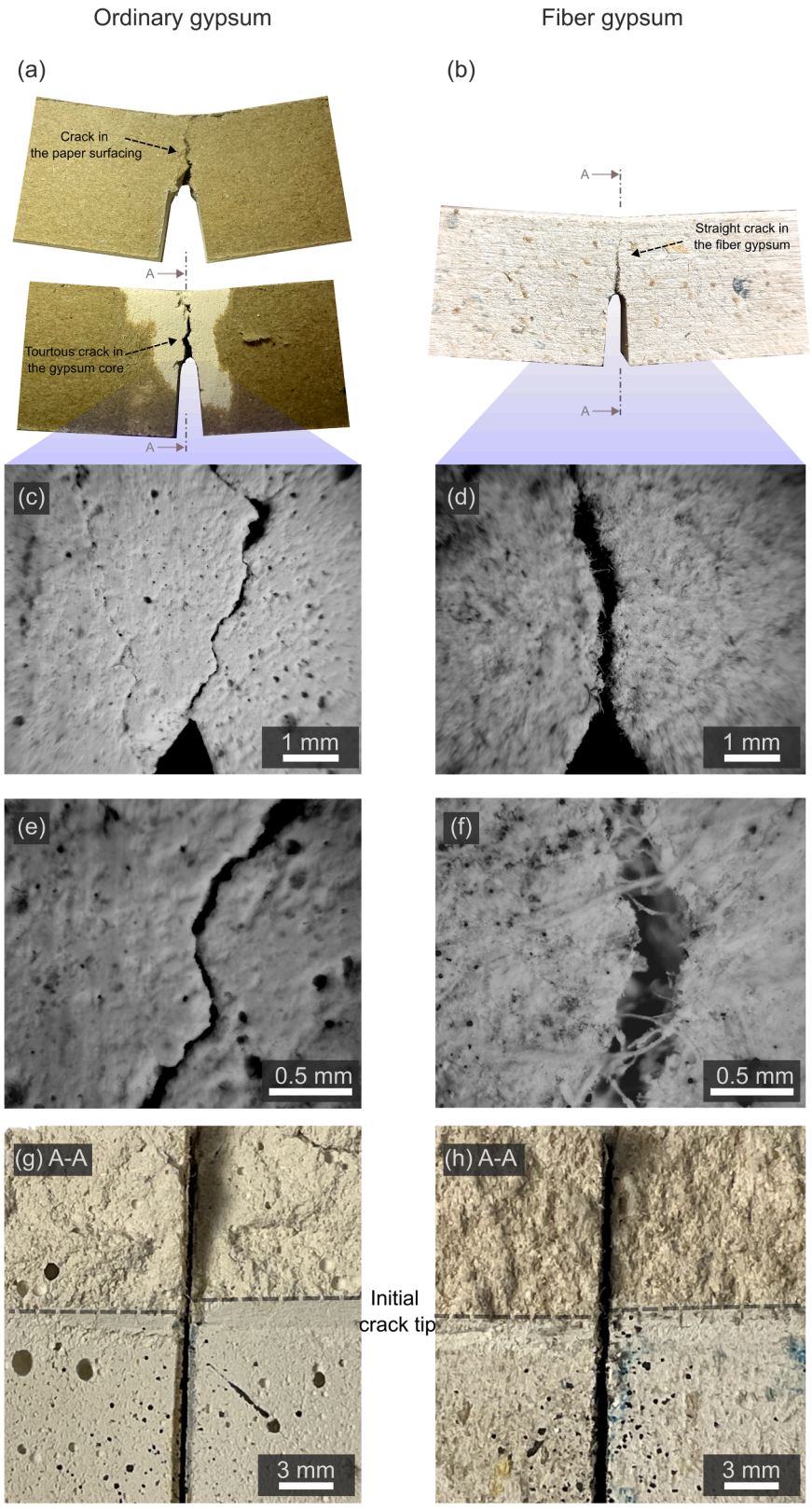

Fig. 10. Frontal photographs (a-b) of the cracked samples, optical micrographs of the crack path (c-d) as well as the crack tips (e-f). Photographs of the cracked surfaces (g-h); the left column is the ordinary gypsum board and the right is the fiber gypsum board from the setup I.

top plywood spacer. With the cracked free surface of the first crack already formed, the vertical displacement was then induced at the right tip of the plywood to the samples, similarly to cantilever beams. Thereafter, the second crack was formed in both materials.

For the FE simulations, the elastic moduli were primarily calibrated with the initial stiffness in Table 1. The modulus of the fiber gypsum board ($E = 1500$ MPa) was much higher than of ordinary gypsum board ($E = 850$ MPa). The tensile strength, estimated with the fundamental

Eq. (2), was higher for the fiber gypsum board ($\sigma_{max} = 4.7$ MPa) than for the ordinary gypsum board ($\sigma_{max} = 2.5$ MPa), obviously because of the difference in peak forces. For the tensile strength of commercial gypsum plasterboards, Petrone et al. [48] found $\sigma_{max} = 1.9$ MPa ($\rho = 720$ kg/m^3) and Martins Irbe et al. [49] (same commercial boards as this work) found $\sigma_{max} = 2.1$ MPa, which is similar figures of the tensile strength of the ordinary gypsum board found here. The tensile strength of the fiber gypsum board was also similar to the previous study. For example, Klöck and Aicher [36] reported $\sigma_{max} \approx 5$ MPa for fiber gypsum specimens reinforced with recycled cellulose fibers (same density and fiber content as in this work). Comparing to other types of fiber gypsum materials, Désiré Omgba Betené et al. [50] reported $\sigma_{max} = 4.5$ MPa for glass fiber gypsum composites ($\rho = 1014$ kg/m^3) and $\sigma_{max} = 2.1$–3.1 MPa for plant fiber gypsum composites ($\rho = 990$–1015 kg/m^3), which are slightly lower figures compared to the fiber gypsum boards in this study.

The tensile softening behavior was assessed by fitting the PF-CZM parameter using FE models to the post-peak forces in the experimental setup I — as observed in Fig. 6(a), the strain hardening at the pre-peak force region is pronounced for ordinary gypsum. In such cases, the tension softening is determined in the post-peak region only [16]. The fitting accuracy was robust ($R^2 \approx 1$) for both materials for the values of the fracture toughness G_c and of PF-CZM parameters a_1, a_2 and p in Table 2. Given the noticeable difference in areas under the curves between the materials in Fig. 6(a), the fracture toughness of the fiber gypsum board ($G_c = 800$ J/m^2) was twice as higher as of the ordinary gypsum board ($G_c = 400$ J/m^2). Normally the fracture toughness of gypsum materials is quite low, e.g., $G_c = 10$–30 J/m^2 from references [8, 51–53]. The high fracture toughness of the ordinary gypsum board compared to neat gypsum materials is because of the major contribution of the paper surfacing during the fracture process and therefore the reported value in this work is an effective value of the entire board; the fracture toughness index of paper liners is about $G_c/\rho = 5$–11 Jm/kg [54].

The fracture toughness of the fiber gypsum board was slightly higher than values found by Aicher and Rüdiger for a recycled fiber gypsum material ($G_c = 660$ J/m^2) [55]. Their experimental tests without an initial notch and lower displacement speed could have caused the difference, but still, the measured values are in the same order of magnitude. The measured value is also comparable to values of other natural fiber gypsum materials, such as a gypsum matrix reinforced with palm fibers with the same fiber content ($G_c = 890$ J/m^2) [56]. Comparing to synthetic fiber gypsum materials, for example, Suárez et al. [53] found $G_c = 752$ J/m^2 and Nguyen et al. [8] $G_c = 400$ J/m^2 for polypropylene fiber gypsum. Wang et al. [57] found $G_c = 481$ J/m^2 for polyethylene fiber gypsum materials; the recycled fiber gypsum board here thus shows equivalent fracture toughness as synthetic fiber gypsum materials. It is also important to mention that there may be influences of manufacturing processes as the samples in the referred works were produced in laboratory size facilities, while the fiber gypsum board in the present work is produced in production scale facilities.

Furthermore, for the shape of the tension softening behavior, the PF-CZM parameter a_2 was higher for the ordinary gypsum board. As depicted in Fig. 4, higher values of a_2 means steeper drop after peak force. The PF-CZM exponent p was also higher for ordinary gypsum, which means an abrupt transition in force; the low values of a_2 and p of the fiber gypsum board are attributed to the fiber bridging mechanism (conf. Fig. 10 (f)). The final fracture softening law are then illustrated in Fig. 8 where the Eqs. (5) and (6) were computed with inputs from Table 2. The critical opening can be estimated as $\Delta_n \approx 0.6$ mm when the tractions become less than 5 percent of the tensile strength. Fig. 8 essentially illustrates the closure tractions as a function of the crack opening for the tension softening behavior of the studied materials. The idealized fracture process zone is relevant to be incorporated in FE structural simulations of timber modules [12].

3.3. Porosity and fractography

Tomography scans are presented in Fig. 9 where the 3D volumes corresponded to a size $12.5 \times 12.5 \times 25$ mm^3 for both materials where the average of voxel size was ≈ 7 μm. Fig. 9 also shows slices from the middle of the scans where high density of pores (black features) is notably more perceptible in the ordinary gypsum board than in the fiber gypsum board. The fiber incorporation associated with the pressing makes the fiber gypsum denser and the different phases (e.g., gypsum and fibers) are more difficult to be distinguished. However, in the 3D scans of the fiber gypsum material, there were some smooth gradient transitions from grey to black, which were the source of calculated porosity. As the fibers are not straight and randomly distributed, this transition may indicate that porous are placed and formed between the fibers and the gypsum phase. From all this, as no clear differences were found in the void size distribution, it was decided to use the average porosity as the reference parameter, understood as the volume fraction of voids respecting the total analyzed. By using the 3-method in the scans, it calculated an average porosity of 28 % for ordinary gypsum and 19 % for fiber gypsum, which are also reported in Table 1.

Details relative to the crack path, as well as photography of the fracture surface, are presented in Fig. 10. It can be observed that ahead of the initial the crack, the crack path of the ordinary gypsum board is tortuous while, in the fiber gypsum board, it is straighter (see, Fig. 10 (a-d)). The tortuous path is because the crack tends to propagate and kink on pores; the uneven fracture surface through the thickness of samples indicates the kinking mechanism (see, uneven fracture surfaces in Fig. 10 (g-h)). On the other hand, the fiber gypsum board does not have that freedom for the crack to propagate just on tine pores and therefore the crack propagation needs to be associated with the fibers behavior, which sew the crack in a certain way that obliges it to propagate straighter as a result of a lower dependence on the pores (Fig. 10 (d, f)). In both materials, the gypsum phase fractured in a similar way, but, in the material with fibers, fiber bridging took place as the toughness mechanism ruling the process (see, the fracture near the crack tip for both materials in Fig. 10 (e-f)) [21].

The fracture surfaces of samples from experimental setups I and II were very similar and, in the following, the discussion is limited between materials only. Fig. 11 presents close-up images of fracture surfaces by SEM of both materials. In original gypsum, the fracture surface reveals the presence of pores with multiple sizes (Fig. 11 (a, c, e, g)) of dimensions from around 10 μm up to ≈ 600 μm in diameter; the pores are randomly distributed as well as their sizes as clearly presented in Fig. 11 (a, c), for instance. The microstructure of the gypsum in the surface of the pores showed rod-shaped particles with length ranging 5–10 μm

Table 2
Material parameters used in the FE simulations.

Material	Elastic modulus E [MPa]	Tensile strength σ_{max} [MPa]	Fracture toughness G_c [J/m^2]	PF-CZM Parameter 1 a_1 [-]	PF-CZM Parameter 2 a_2 [-]	PF-CZM exponent p [-]	Coefficient of determination R^2 [-]
Ordinary gypsum	850	2.5	400	146	3.5	5.5	0.985
Fiber gypsum	1500	4.7	800	265	1.5	4.0	0.998

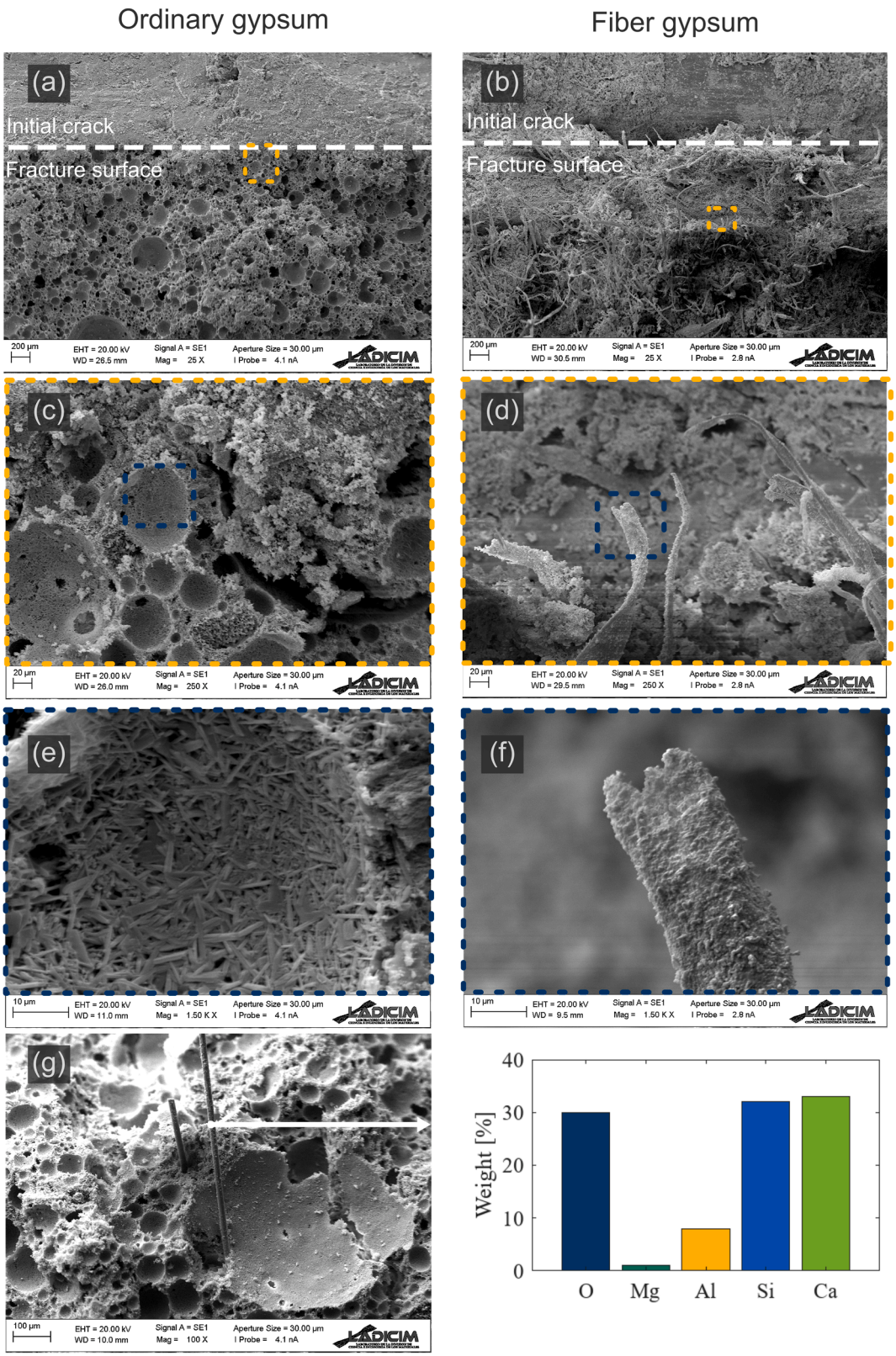

Fig. 11. Close-up micrographs of the fracture surfaces of original gypsum (left) and fiber gypsum(right). Details are revealed of the pores and paper fibers showing near the crack tip; the small boxes in dashed lines refer to high-magnification images in the next row.

approximately (c.f. Fig. 11 (e)). The small rods are gypsum crystals [58]. In addition, other fibers were found in the ordinary gypsum with higher aspect ratio and in low density distribution shown in Fig. 11 (g), which are pointed with a white arrow. According to a semiquantitative analysis presented in the bars graph on Fig. 11, those are based on Si and Ca oxides indicating they are glass fibers. For ordinary gypsum used, the production process is mixed with some additives, which some of them are glass fibers according to the supplier specifications.

In the fiber gypsum material, the paper fibers are tangled and uniformly spread throughout the fracture surface as shown in Fig. 11 (b). Fig. 11 (d, f) shows a single fiber nearly intact with some fine particles of gypsum on it, which suggests the fiber pull-out as the main failure mechanism during the fracture process. The fiber has the width of ≈ 15 μm, which is typically the dimension reported in the literature [34, 35].

4. Conclusion

The fracture properties and behaviour of fiber gypsum and ordinary gypsum commercial plasterboards used in timber modules were assessed under the presented four-point single-edge-notched bending tests and PF-CZM simulations. The tests were also complemented with tomography for porosity measurements and microscopy for fracture surface examinations.

From the fracture tests in the load-crack effective opening curves before the crack growth, the fiber gypsum board were stiffer with an elastic modulus of twice as large as of the ordinary gypsum board. The fiber gypsum board is also stronger than ordinary gypsum with tensile strength twice as higher. Better mechanical performance of the fiber gypsum board is attributed to high bulk density ($\approx 2\times$) and porosity of 30 % lower compared to the tested ordinary gypsum boards. In addition, a larger non-linear behaviour prior to the peak force was found in ordinary gypsum than in fiber gypsum, which may have caused due to significant amount of porous in it and ductility of their paper surfacing.

From the complete fracture tests, the post-peak force response for both materials were tail-like softening curves, typically seen in cementitious materials. PF-CZM fitted well the shape of tension softening curves with the experiments for both materials. The less steep drop in the curves for fiber gypsum was also captured by the low values of the exponent p and parameter a_2. Once calibrated, the model could also predict the shear crack and secondary crack induced by the wooden spacer in the asymmetric tests. As a result of the calibrated model, the fracture toughness of the fiber gypsum board ($= 800$ J/m^2) was predicated as twice as higher as of the ordinary gypsum board ($= 400$ J/m^2). The measured fracture toughness of the fiber gypsum board is comparable with the literature values of other gypsum composites reinforced with natural and synthetic fibers. For the ordinary gypsum board, there has been a great contribution of the paper liners, which was the reason of high fracture toughness compared to literature values of neat gypsum materials. The shape of tension softening curves of the ordinary gypsum board can also be attributed to the paper surfacing.

For the tomography analysis, the fiber incorporation makes observations of different phases more difficult, but clearly showed the porous in the ordinary gypsum board. μTAC scans revealed higher porosity ($=$ 28 %) in the ordinary gypsum board than in the fiber gypsum board ($=$ 19 %). No well-defined porous were detected in the scans of the fiber gypsum board, but the grayscale transition regions may indicate that porous are located between the fibers and the gypsum phase. Fracture surfaces from post-mortem fractography shows similar brittle fracture in the gypsum phase for both materials, but the fracture mechanism of fiber gypsum was different. From the micrographs, it indicates the fiber bridging mechanism provided by the fibers, with final pull-out of them. The difference between experimental setup I and II in both materials seems to be macroscopic, and it is related with the orientation of the crack plane propagation (45º in II). From optical micrographs at the front view, the crack path of ordinary gypsum was tortious because the crack propagates and kinks in the porous medium. The crack path of fiber gypsum was slightly straighter than ordinary gypsum.

The primarily efforts of this work in collecting non linear quasi brittle fracture properties, such as tensile strength, fracture toughness and traction-separation laws, is materialized in Table 2 and Fig. 8, which will be essential material parameters in the structural FE models of timber modules to predict unwanted crack initiation and propagation at the corners of door openings. In addition, the present work provides results of fracture mechanisms and the porosity-mechanical properties relation of gypsum composites that lacks being reported for commercial plasterboards. There has been a great effort in the research community to develop sustainable gypsum composites reinforced with different fibers. In this respect, the reported findings in this work are key and can be seen as reference values for developing new gypsum materials in comparison with commercial gypsum plasterboards having a well-defined application (timber modules). However, we point out that our values are limited to quasistatic tests and recommend further investigations on how the fracture properties are affected by rate dependence, especially for the fiber gypsum board.

CRediT authorship contribution statement

Marcus Vinícius Tavares da Costa: Writing – review & editing, Writing – original draft, Methodology, Investigation, Formal analysis, Data curation, Conceptualization. **Sergio Cicero:** Writing – review & editing, Writing – original draft, Methodology, Formal analysis, Data curation. **Borja Arroyo:** Writing – review & editing, Writing – original draft, Investigation, Formal analysis, Data curation.

Declaration of Competing Interest

The authors declare that they have no known competing financial interests or personal relationships that could have appeared to influence the work reported in this paper.

Acknowledgements

Derome AB is acknowledged for supplying the materials. The authors are grateful for the research funding from the Knowledge Foundation (KKS), KK project number 20210063. Eng. Lars Pettersson is acknowledged for manufacturing the bending rig as well as the engineering students from Karlstad University Mr. Mattias Edvinsson, Mr. Hugo Wittemyr and Ms. Andréa Truffert for their assistance in the experimental tests. Dr. Johan Vessby is also acknowledged for revision of the manuscript and valuable advice on the problem in timber modules. MVTdC acknowledges the KAU Travel grant for the collaboration within EUNICE alliance.

Data Availability

Data will be made available on request.

References

[1] M.T. Esan, Review of gypsum reinforced composites as building materials, Discov. Civ. Eng. 1 (1) (2024).
[2] J. Skujans, A. Vulans, U. Iljins, A. Aboltins, Measurements of heat transfer of multi-layered wall construction with foam gypsum, Appl. Therm. Eng. 27 (7) (2007) 1219–1224.
[3] F. Hernández-Olivares, M.R. Bollati, M. del Rio, B. Parga-Landa, Development of cork–gypsum composites for building applications, Constr. Build. Mater. 13 (4) (1999) 179–186.
[4] F. Alfawakhiri, M.A. Sultan, D.H. MacKinnon, Fire resistance of loadbearing steel-stud wall protected with gypsum board: a review, Fire Technol. 35 (1999) 308–335.
[5] A. Erbs, A. Nagalli, K. Querne de Carvalho, V. Mymrin, F.H. Passig, W. Mazer, Properties of recycled gypsum from gypsum plasterboards and commercial gypsum throughout recycling cycles, J. Clean. Prod. 183 (2018) 1314–1322.
[6] L. Boquera, E. Olacia, C. Fabiani, A.L. Pisello, A.D. Alessandro, F. Ubertini, L. F. Cabeza, Thermo-acoustic and mechanical characterization of novel bio-based plasters: the valorisation of lignin as by-product from biomass extraction for green building applications, Constr. Build. Mater. 278 (2021) 122373.
[7] F. Nindiyasari, E. Griesshaber, T. Zimmermann, A.P. Manian, C. Randow, R. Zehbe, L. Fernandez-Diaz, A. Ziegler, C. Fleck, W.W. Schmahl, Characterization and mechanical properties investigation of the cellulose/gypsum composite, J. Compos. Mater. 50 (5) (2016) 657–672.
[8] H. Nguyen, P. Kinnunen, V. Carvelli, M. Mastali, M. Illikainen, Strain hardening polypropylene fiber reinforced composite from hydrated ladle slag and gypsum, Compos. Part B: Eng. 158 (2019) 328–338.

[9] M. Hošťálková, N. Vavřínová, V. Longauerová, Mechanical properties of the gypsum composite reinforcement with wooden fibers, Int. Rev. Appl. Sci. Eng. 10 (1) (2019) 15–21.
[10] Swedish Wood, Design of Timber Structures: Structural Aspects of Timber Construction, Swedish Wood, 2022.
[11] R. Maharjan, L. Kuai, J. Vessby, S. Ormarsson, An experimental analysis of full scale light-frame timber modules, Eng. Struct. 304 (2024) 117617.
[12] L. Kuai, R. Maharjan, S. Ormarsson, J. Vessby, Numerical and experimental investigations of cracked light-frame timber walls, J. Build. Eng. 96 (2024) 110507.
[13] B.L. Karihaloo, Fracture Mechanics & Structural Concrete, Pearson Education, 1995.
[14] T.L. Anderson, Fracture Mechanics: Fundamentals and Applications, CRC Press, 2017.
[15] J.-Z. Zhang, X.-P. Zhou, Fracture process zone (FPZ) in quasi-brittle materials: review and new insights from flawed granite subjected to uniaxial stress, Eng. Fract. Mech. 274 (2022) 108795.
[16] H. Cornelissen, D. Hordijk, H. Reinhardt, Experimental determination of crack softening characteristics of normalweight and lightweight, Heron 31 (2) (1986) 45–46.
[17] A. Hillerborg, M. Modéer, P.E. Petersson, Analysis of crack formation and crack growth in concrete by means of fracture mechanics and finite elements, Cem. Concr. Res. 6 (6) (1976) 773–781.
[18] G.I. Barenblatt, The mathematical theory of equilibrium cracks in brittle fracture, Elsevier, 1962, pp. 55–129.
[19] D.S. Dugdale, Yielding of steel sheets containing slits, J. Mech. Phys. Solids 8 (2) (1960) 100–104.
[20] M. Elices, G.V. Guinea, J. Gómez, J. Planas, The cohesive zone model: advantages, limitations and challenges, Eng. Fract. Mech. 69 (2) (2002) 137–163.
[21] M.E. Launey, R.O. Ritchie, On the fracture toughness of advanced materials, Adv. Mater. 21 (20) (2009) 2103–2110.
[22] E. Jungstedt, M.V. Tavares da Costa, S. Östlund, L.A. Berglund, On the high fracture toughness of wood and polymer-filled wood composites – Crack deflection analysis for materials design, Eng. Fract. Mech. 300 (2024) 109994.
[23] E. Jungstedt, M.V. Tavares da Costa, S. Östlund, L.A. Berglund, Fracture toughness of wood and transparent wood biocomposites in the toughest LT-direction, Mater. Des. 231 (2023) 112058.
[24] E. Jungstedt, S. Östlund, L.A. Berglund, Transverse fracture toughness of transparent wood biocomposites by FEM updating with cohesive zone fracture modeling, Compos. Sci. Technol. 225 (2022) 109492.
[25] C. Miehe, M. Hofacker, F. Welschinger, A phase field model for rate-independent crack propagation: Robust algorithmic implementation based on operator splits, Comput. Methods Appl. Mech. Eng. 199 (45) (2010) 2765–2778.
[26] B. Bourdin, G.A. Francfort, J.J. Marigo, Numerical experiments in revisited brittle fracture, J. Mech. Phys. Solids 48 (4) (2000) 797–826.
[27] M. Cervera, G.B. Barbat, M. Chiumenti, J.Y. Wu, A comparative review of XFEM, mixed FEM and phase-field models for quasi-brittle cracking, Arch. Comput. Methods Eng. 29 (2) (2022) 1009–1083.
[28] J.-Y. Wu, A unified phase-field theory for the mechanics of damage and quasi-brittle failure, J. Mech. Phys. Solids 103 (2017) 72–99.
[29] J.-Y. Wu, Robust numerical implementation of non-standard phase-field damage models for failure in solids, Comput. Methods Appl. Mech. Eng. 340 (2018) 767–797.
[30] Y. Navidtehrani, C. Betegón, E. Martínez-Pañeda, A unified Abaqus implementation of the phase field fracture method using only a User Material Subroutine, Materials 14 (8) (2021) 1913.
[31] R.A. Muñetón-López, O. Giraldo-Londoño, A phase-field formulation for cohesive fracture based on the Park–Paulino–Roesler (PPR) cohesive fracture model, J. Mech. Phys. Solids 182 (2024) 105460.
[32] Knauf Danogips GmbH, Environmental product declaration (EPD) for plasterboards from Knauf Danogips GmbH, 2025. ⟨https://knauf.com/sv-SE⟩. (Accessed 2025).
[33] Fermacell, Orange book, Fermacell (2016).
[34] T. De Assis, J. Pawlak, L. Pal, H. Jameel, R. Venditti, L.W. Reisinger, D. Kavalew, R. W. Gonzalez, Comparison of wood and non-wood market pulps for tissue paper application, BioResources 14 (3) (2019) 6781–6810.
[35] F. Drolet, T. Uesaka, A stochastic structure model for predicting sheet consolidation and print uniformity, Adv. Pap. Sci. Technol. (2005) 1139–1154.
[36] W. Klöck, S. Aicher, Size effect in paper fiber-reinforced gypsum panels under in-plane bending, Wood Fiber Sci. (2005) 403–412.
[37] M.Y. He, J.W. Hutchinson, Asymmetric four-point crack specimen, J. Appl. Mech. 67 (1) (1999) 207–209.
[38] J.B. Jørgensen, C. Kildegaard, B.F. Sørensen, Design of four-point SENB specimens with stable crack growth, Eng. Fract. Mech. 191 (2018) 168–186.
[39] E. Linul, L. Marsavina, D.I. Stoia, Mode I and II fracture toughness investigation of Laser-Sintered Polyamide, Theor. Appl. Fract. Mech. 106 (2020) 102497.
[40] E. Schlangen, Experimental and numerical analysis of fracture processes in concrete, Heron 38 (1993) 1–17.
[41] E1820, Standard test method for measurement of fracture toughness, ASTM International, West Conshohocken.
[42] T. Wang, Y. Wang, R. Crocetti, M. Wålinder, Influence of face grain angle, size, and moisture content on the edgewise bending strength and stiffness of birch plywood, Mater. Des. 223 (2022) 111227.
[43] I. Soroka, P.J. Sereda, Interrelation of hardness, modulus of elasticity, and porosity in various gypsum systems, J. Am. Ceram. Soc. 51 (6) (1968) 337–340.
[44] J. Sainz-Aja, I. Carrascal, J.A. Polanco, C. Thomas, Fatigue failure micromechanisms in recycled aggregate mortar by μCT analysis, J. Build. Eng. 28 (2020) 101027.
[45] J. Santa Cruz Astorqui, M. Del Río Merino, P. Villoria Sáez, C. Porras-Amores, Analysis of the relationship between density and mechanical strength of lightened gypsums: Proposal for a coefficient of lightening, Adv. Mater. Sci. Eng. 2017 (2017) 1–7.
[46] S. Östlund, K. Niskanen, Mechanics of Paper Products, De Gruyter, 2021.
[47] R. Malm, Shear cracks in concrete structures subjected to in-plane stresses, Trita-BKN, KTH, Bulletin, 2006, p. 136 (pp. xii,).
[48] C. Petrone, G. Magliulo, G. Manfredi, Mechanical properties of plasterboards: experimental tests and statistical analysis, J. Mater. Civ. Eng. 28 (11) (2016) 04016129.
[49] J.V. Martins Irbe, M. Cerpinska, V. Beresnevics, K. Spade, Study of flexural and yield strength of gypsum composite boards, International Scientific Conference Engineering for Rural Development, Jelgava, Latvia, 2023.
[50] A. Désiré Omgba Betené, F. Martoïa, P.J.J. Dumont, F. Ebanda Betené, A. Ateba, Gypsum plaster composites reinforced with tropical fibre bundles extracted from Rhecktophyllum camerunense and Ananas comosus plants: Microstructure and mechanical performance, Constr. Build. Mater. 392 (2023) 131815.
[51] D. Pietras, M.R.M. Aliha, H.G. Kucheki, T. Sadowski, Tensile and tear-type fracture toughness of gypsum material: Direct and indirect testing methods, J. Rock. Mech. Geotech. Eng. 15 (7) (2023) 1777–1796.
[52] A. Doitrand, R. Henry, S. Meille, Brittle material strength and fracture toughness estimation from four-point bending test, J. Theor., Comput. Appl. Mech. (2021).
[53] F. Suárez, L. Felipe-Sesé, F.A. Díaz, J.C. Gálvez, M.G. Alberti, On the fracture behaviour of fibre-reinforced gypsum using micro and macro polymer fibres, Constr. Build. Mater. 244 (2020) 118347.
[54] P. Mäkelä, C. Fellers, An analytic procedure for determination of fracture toughness of paper materials 27 (2) (2012) 352–360.
[55] S. Aicher, F. Rüdiger, Fracture characterization of cellulose fiber gypsum composite subject to inplane tension loading, Otto-Graf. -J. 15 (2004) 91.
[56] A. Sahraoui, T. Djoudi, M. Hecini, Investigating the impact of date palm fiber waste on the properties of a novel gypsum-based bio-composite, Constr. Build. Mater. 457 (2024) 139419.
[57] Y. Wang, J. Song, Z. Hu, Y. Zhang, Z. Guan, H. Yang, Mechanical and water resistance properties of strain hardening fiber reinforced gypsum-based composites, Constr. Build. Mater. 425 (2024) 136116.
[58] A.P. Fantilli, D. Jóźwiak-Niedźwiedzka, P. Denis, Bio-fibres as a reinforcement of gypsum composites, Materials 14 (17) (2021) 4830.